

**Experimental study of a freely falling plate with an inhomogeneous mass distribution**Wentao Huang,<sup>1</sup> Hong Liu,<sup>1</sup> Fuxin Wang,<sup>1</sup> Junqi Wu,<sup>1</sup> and H. P. Zhang<sup>2,\*</sup><sup>1</sup>*J. C. Wu Center for Aerodynamics and School of Aeronautics and Astronautics, Shanghai Jiao Tong University, China*<sup>2</sup>*Department of Physics and Astronomy and Institute of Natural Sciences, Shanghai Jiao Tong University, China*

(Received 17 April 2013; revised manuscript received 20 September 2013; published 11 November 2013)

A homogeneous thin plate often flutters while falling through a fluid under gravity. The center of gravity of the plate moves back-and-forth horizontally and the plate tilting angle oscillates symmetrically from the horizontal. Here we show that such a scenario is qualitatively changed for a plate with noncoinciding centers of gravity and buoyancy due to an inhomogeneous mass distribution. Mismatch of the centers causes an external torque that breaks the symmetry of rotational motion, shifts the mean tilting position from the horizontal, and leads to a net horizontal plate displacement. In laboratory experiments with a Reynolds number around 1500, we found that the net horizontal displacement scales linearly with the separation between the centers up to a critical value, beyond which the plate falls vertically in an edge-on configuration with the heavier side downward. Experimental results are compared to predictions of a quasi-steady numerical model. Our work demonstrates that motion of freely moving objects in a fluid depends sensitively on external torques, which potentially can be used as an effective control method.

DOI: [10.1103/PhysRevE.88.053008](https://doi.org/10.1103/PhysRevE.88.053008)

PACS number(s): 47.20.Ib, 47.20.Ky, 47.27.wb

**I. INTRODUCTION**

When a leaf falls from a tree, its trajectory is often not straight but exhibits complex dynamics. Understanding and predicting such falling trajectories have impacts in a broad range of fields [1], such as meteorology [2], sedimentology [3], and biomechanics [4,5]. Studies of the subject have a long history starting with Maxwell [6] who provided a qualitative description for tumbling motion. Kirchhoff theoretically considered motion of a solid body in an inviscid fluid [7] and demonstrated that the inertial interaction of the liquid with the moving solid can be quantified by a renormalized added mass tensor and that the motion of the body can be described by a set of ordinary differential equations [8–11]. The inviscid theory misses two crucial ingredients: viscous drag and vorticity, both of which are related to the motion of the body in a complex manner. Therefore, a general analytical description of a falling body in a viscous fluid has not been obtained. To investigate this problem, researchers have turned to experiments [12–20], numerical simulations [21–26], and phenomenological models [17,27,28].

To reduce the complexity of the problem, many previous studies [15–17,27] focused on thin quasi-two-dimensional plates. Centers of gravity of these plates falls within a vertical plane and exhibit at least three kinds of nonchaotic motion: steady vertical descent, oscillatory flutter, and rotary tumbling. At low Reynolds numbers, the flow around the plate is symmetric and the plate falls vertically. As the Reynolds number increases, more complex trajectories emerge. A thin plate with a large width-to-thickness ratio flutters: plate tilting angle oscillates symmetrically from the horizontal and the center of mass moves back and forth horizontally, producing no mean horizontal displacement. As the width-to-thickness ratio decreases, the plate transits from fluttering to tumbling motion, in which the plate undergoes full end-over-end rotation and

drifts horizontally. The three kinds of motion and transitions between them have been studied extensively [15–17,29–31]. Plates in these previous studies all have a homogeneous mass distribution; this leads the centers of buoyancy and gravity to coincide and therefore the two forces produce zero net torque.

In this paper, we investigate how the fluttering dynamics of a plate is changed if an external torque is introduced by offsetting the centers of gravity and buoyancy. Through laboratory experiments and a quasi-steady numerical model, we show that torque generated by an offset as small as a few thousandth of the plate width can shift the mean tilting position from the horizontal and lead to a net horizontal plate displacement, therefore qualitatively changing the falling dynamics. We further show that the net horizontal displacement scales linearly with the separation between the centers up to a critical value, beyond which the plate falls vertically in an edge-on configuration with the heavier side downward.

The paper is organized as follows. In Sec. II we describe the experimental setup and the quasi-steady numerical model. The main results of this work are given in Sec. III and we summarize our results in Sec. IV.

**II. EXPERIMENT AND MODEL****A. Experimental setup**

Experiments are performed in a glass tank (1 m × 0.5 m × 0.5 m) that is filled of water seeded with 10 μm TiO<sub>2</sub> tracer particles, as shown in Fig. 1. Plates are held and released by a robotic hand mounted at the top of the tank. Upon releasing, plates fall with two-dimensional trajectories in the XY plane. Motion of the plates and TiO<sub>2</sub> tracer particles in a vertical (XY) plane is illuminated by a light-sheet and recorded by a camera with a resolution of 512 pixels × 512 pixels that runs at 50 frames/s. Images are analyzed in Matlab to extract the plate motion. Fluid flow is quantified by applying a particle image velocimetry algorithm to the images of tracer particles. Plates are released from rest with an initial tilt angle  $\theta = 0$  [defined in Fig. 2(b)]. In most of our experiments, plates exhibit periodic motion that is insensitively dependent on the small

\*Author to whom correspondence should be addressed: [hepeng\\_zhang@sjtu.edu.cn](mailto:hepeng_zhang@sjtu.edu.cn)

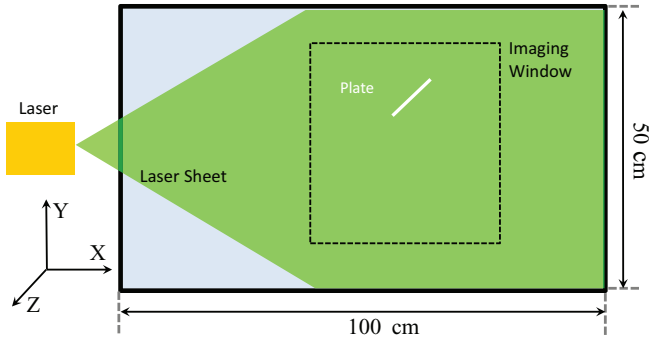


FIG. 1. (Color online) Front view of the experimental system showing the falling plate, the illuminating light-sheet, and the imaging window. A laboratory reference frame ( $XYZ$ ) is fixed in space with  $Y$  axis pointing vertically and other two horizontally. The light-sheet lies in the  $XY$  plane.

variations of the initial tilt angle. We perform measurements in the center region of the tank to minimize the influences of the tank boundaries.

Plates are quasi-two-dimensional and the longest dimension along the  $Z$  direction is 25 cm. Results are checked against additional experiments performed with a longer plate (35 cm) to ensure that end effects are negligible. A schematic drawing of the plate's  $XY$  cross-section is shown in Fig. 2(a). To construct a plate, we start with a piece of plastic (acrylic) with a cross section of  $a \times b$  and a center at  $O'$  which is called the center of (exterior) geometry or buoyancy. Part of the acrylic

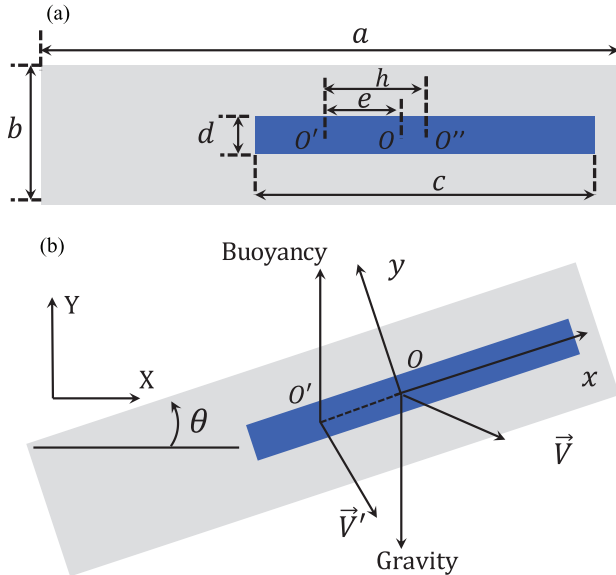


FIG. 2. (Color online) (a) Construction of the plates. Two materials (distinguished by colors) with different densities are used to construct the plate. Geometric parameters are defined in the text. (b) A comoving frame ( $xy$ ) is fixed on the plate and follows the plate motion. The moving frame has its origin at the center of gravity of the plate, denoted as  $O$ , and its two axes are along and perpendicular to the plate orientation that is quantified by a tilting angle  $\theta$  from the horizontal. The center of exterior geometry, i.e., the center of buoyancy, is denoted by  $O'$ . The centers of gravity and buoyancy have velocities of  $\vec{V}$  and  $\vec{V}'$ , respectively.

TABLE I. Geometric parameters of two sets of plates. Definitions of symbols are given in the text and Fig. 2.

	$a$ (cm)	$b$ (cm)	$c$ (cm)	$d$ (cm)	$e/a$
Set A	2.5	0.3	1	0.1	[0,0.02]
Set B	3.0	0.3	1.2	0.1	[0,0.02]

plate is milled off and replaced by an aluminum plate with a cross section of  $c \times d$ ; the aluminum plate is centered at  $O''$  which is horizontally displaced from  $O'$  by  $h$ .

The mass (per unit length along  $Z$  direction) of the composite plate is

$$m = \rho_p ab + (\rho_a - \rho_p)cd, \quad (1)$$

where  $\rho_p = 1.2 \text{ g/cm}^3$  and  $\rho_a = 2.7 \text{ g/cm}^3$  are densities for plastic and aluminum. The center of gravity of the plate is denoted as  $O$  and the offset of  $O$  from  $O'$  is

$$e = \frac{(\rho_a - \rho_p)cd}{m}h. \quad (2)$$

The moment of inertia with respect to the axis through  $O$  into the plate is

$$I = \rho_p ab \left( \frac{a^2 + b^2}{12} + e^2 \right) + (\rho_a - \rho_p)cd \left( \frac{c^2 + d^2}{12} + (h - e)^2 \right). \quad (3)$$

Two different sets of plates are used in experiments. As shown in Table I, in each set, plates have the same parameters of  $a$ ,  $b$ ,  $c$ , and  $d$  but different offset  $e$ , which ranges from 0 to two percent of the width  $a$ . By varying  $e$ , we can systematically change the net torque produced by the gravity and buoyancy.

## B. Quasi-steady model

Building on Kirchhoff's theory of a solid moving in an inviscid fluid, Wang *et al.* proposed a quasi-steady model to describe the falling dynamics of homogeneous plates [17,21,29]. The model can be conveniently expressed in a frame comoving with the plate, the  $xy$  frame in Fig. 2(b). The moving frame has its origin at the center of gravity of the plate and its two axes are along and perpendicular to the plate orientation, respectively. As shown in Fig. 2(b), the plate tilts with an angle of  $\theta$  with respect to the horizontal. The instantaneous velocities for the centers of gravity and buoyancy are  $\vec{V} = u\vec{i} + v\vec{j}$  and  $\vec{V}' = u'\vec{i} + v'\vec{j}$ ; they are related by

$$\vec{V}' = \vec{V} - (e\dot{\theta})\vec{j}. \quad (4)$$

The plate dynamics is governed by the following coupled ordinary differential equations expressed in the co-moving frame:

$$(m + m_{11})\dot{u} = (m + m_{22})\dot{\theta}v - m'g \sin \theta - \rho_f \Gamma v - F_x, \quad (5)$$

$$(m + m_{22})\dot{v} = (m + m_{11})\dot{\theta}u - m'g \cos \theta + \rho_f \Gamma u - F_y, \quad (6)$$

$$(I + I_a)\ddot{\theta} = (m_{11} - m_{22})uv - (\rho_f ab)ge \cos \theta - \tau, \quad (7)$$

where  $\rho_f = 1.0 \text{ g/cm}^3$  is the fluid density,  $g$  is the acceleration of gravity, the buoyancy-corrected mass is  $m' = m - \rho_f ab$ , and  $m_{11}$ ,  $m_{22}$ , and  $I_a$  are added mass coefficients. We estimate the added mass coefficients for a rectangular cylinder by averaging coefficients of two elliptical cylinders that have an inscribed ellipse and a circumscribed ellipse with a minimal area, respectively. Under this approximation, we have

$$\begin{aligned} m_{11} &= \frac{3\pi}{8} \rho_f b^2, & m_{22} &= \frac{3\pi}{8} \rho_f a^2, \\ I_a &= \frac{5\pi}{256} \rho_f (a^2 - b^2) + \frac{3\pi}{8} \rho_f a^2 e^2. \end{aligned} \quad (8)$$

The second (small) term for  $I_a$  reflects the fact that the origin of the comoving  $xy$  frame is set at the center of gravity not at the center of buoyancy [32].

Equation (5) and (6) describe translational motion in the comoving  $xy$  frame. The third and fourth terms on the right-hand side represent aerodynamic lift and drag forces; parametrization of these forces will be discussed in the next paragraph. Rotational dynamics is governed by Eq. (7). The second term on the right-hand side,  $-(\rho_f ab)ge \cos \theta$ , is the torque due to buoyancy force acting at the center of buoyancy; such an external torque does not exist in plates with zero offset  $e = 0$ . The last term in Eq. (7) is the rotational drag. All three degrees of freedom couple with each other through the first terms on the right-hand side of the equations; these terms arise from added-mass effects and from the fact that the  $xy$  frame rotates with an angular velocity of  $\dot{\theta}$ .

Translation and rotation of the plate are also coupled through aerodynamic lift. To parametrize the lift, Wang *et al.* [21,29,33] have used numerical and experimental results to construct a self-consistent form for the circulation around the body,  $\Gamma$ , in terms of the velocity of the center of buoyancy,  $(u', v')$ , and the angular velocity,  $\dot{\theta}$ , as

$$\Gamma = -C_T a \frac{u'v'}{\sqrt{u'^2 + v'^2}} + \frac{1}{2} C_R a^2 \dot{\theta}, \quad (9)$$

where  $C_T$ ,  $C_R$  are nondimensional constants controlling contributions from translation and rotation, respectively. For drag terms, in the regime of the relatively high Reynolds numbers  $\sim O(10^3)$ , Wang *et al.* proposed quadratic drag terms for both translation and rotation:

$$F_x = -\frac{\rho_f a}{2} \left[ C_0 \frac{u'^2}{\sqrt{u'^2 + v'^2}} + C_{\pi/2} \frac{v'^2}{\sqrt{u'^2 + v'^2}} \right] u', \quad (10)$$

$$F_y = -\frac{\rho_f a}{2} \left[ C_0 \frac{u'^2}{\sqrt{u'^2 + v'^2}} + C_{\pi/2} \frac{v'^2}{\sqrt{u'^2 + v'^2}} \right] v', \quad (11)$$

$$\tau = C_\tau \frac{\rho_f a^4 \dot{\theta} |\dot{\theta}|}{64}, \quad (12)$$

where  $C_0$ ,  $C_{\pi/2}$ , and  $C_\tau$  are nondimensional drag coefficients. Wang *et al.* computed the torque produced by drag [Eq. (12)] with respect to the center of buoyancy; a shift of the reference point from the center of buoyancy to the center of gravity in our work leads to a negligible error proportional to  $(e/a)^2$ . As shown in Refs. [17,29], this set of parameters can capture the qualitative behavior of the forces acting on plates during both fluttering and tumbling motion. We note that the circulation in Eq. (9) and drags in Eqs. (10) to (12) depend only on the plate's instantaneous motion and have no history dependence;

TABLE II. Fitting parameters of the quasi-steady model.

	$C_T$	$C_R$	$C_0$	$C_{\pi/2}$	$C_\tau$
Fitting values	4.5	1.8	0.2	0.5	1.9

such a quasi-steady assumption is a great simplification of the full flow-structure interaction problem.

Dynamic equations [Eqs. (5) and (6)], parametrization [Eqs. (9) to (12)], and the kinematic relation [Eq. (4)] form a closed system. For any given set of parameters, we solve the system with a Runge-Kutta algorithm to compute velocities  $(u, v, \theta)$  that can be further integrated to get trajectories. The five parameters ( $C_T$ ,  $C_R$ ,  $C_0$ ,  $C_\pi$ , and  $C_\tau$ ) used in Eqs. (9) to (12) primarily depend on the exterior dimensions of the plates,  $a$  and  $b$  in Fig. 2. Since two sets of plates used in experiments have similar exterior geometry, shown in Table I, we assume that the five parameters have the same values for all plates. A global fit of model predictions to experimental trajectories for all plates leads to parameters shown in Table II. As in experiments, plates in models are released from rest and with an initial tilt angle  $\theta = 0$ .

### III. RESULTS

#### A. Falling trajectories

In the left column of Fig. 3, we plot falling trajectories of the center of gravity of four plates from Set A (cf. Table I); these plates have the same geometric parameters but different offsets. The corresponding model results are plotted in the right column of Fig. 3. In Figs. 3(a) and 3(b), a zero-offset plate with a width-to-thickness ratio  $b/a = 0.12$  and a dimensionless moment of inertia  $I^* = 8\rho_a b(a^2 + b^2)/(3\pi\rho_f a^3) = 0.13$  falls with a mean vertical speed  $V = 6 \text{ cm/s}$ . A Reynolds number can be defined by using the width of the plate and the descent speed:  $\text{Re} = aV/\nu = 1500$ . Since the moment of inertia of the plate,  $I^* = 0.13$ , is less than the critical value 0.2–0.3 characterizing the transition from fluttering to tumbling motion [13,15,29], the plate exhibits fluttering motion which consists of alternating gliding at low angle of attack and fast rotation at the turning points. As it falls, the plate oscillates symmetrically from side to side horizontally. With such a left-right symmetry, fluttering motion produces zero net horizontal motion.

The left-right symmetry can be broken by introducing a nonzero offset. In Fig. 3(c), the center of gravity of the plate is shifted to the right by less than one percent of the plate width ( $e/a = 0.0086$ ) and the consequence is obvious: the plate travels less to the left in each period and drifts to the right for about 20 cm while falling vertically for 35 cm. Increasing the offset leads to larger horizontal displacements, as shown in Fig. 3(e). If the offset is too large, the external torque dominates over other terms in Eq. (7) and forces the plate to fall vertically in an edge-on configuration with the heavier side downward. The initial phase of such a trajectory is shown in Fig. 3(g).

With the parameters in Table I, the quasi-steady model can reproduce trajectories of plates with zero or small offsets as shown in Figs. 3(b), 3(d), and 3(f), but it fails to predict the edge-on vertical descending observed in the plate with  $e/a = 0.0172$ . This inadequacy of the model may arise from

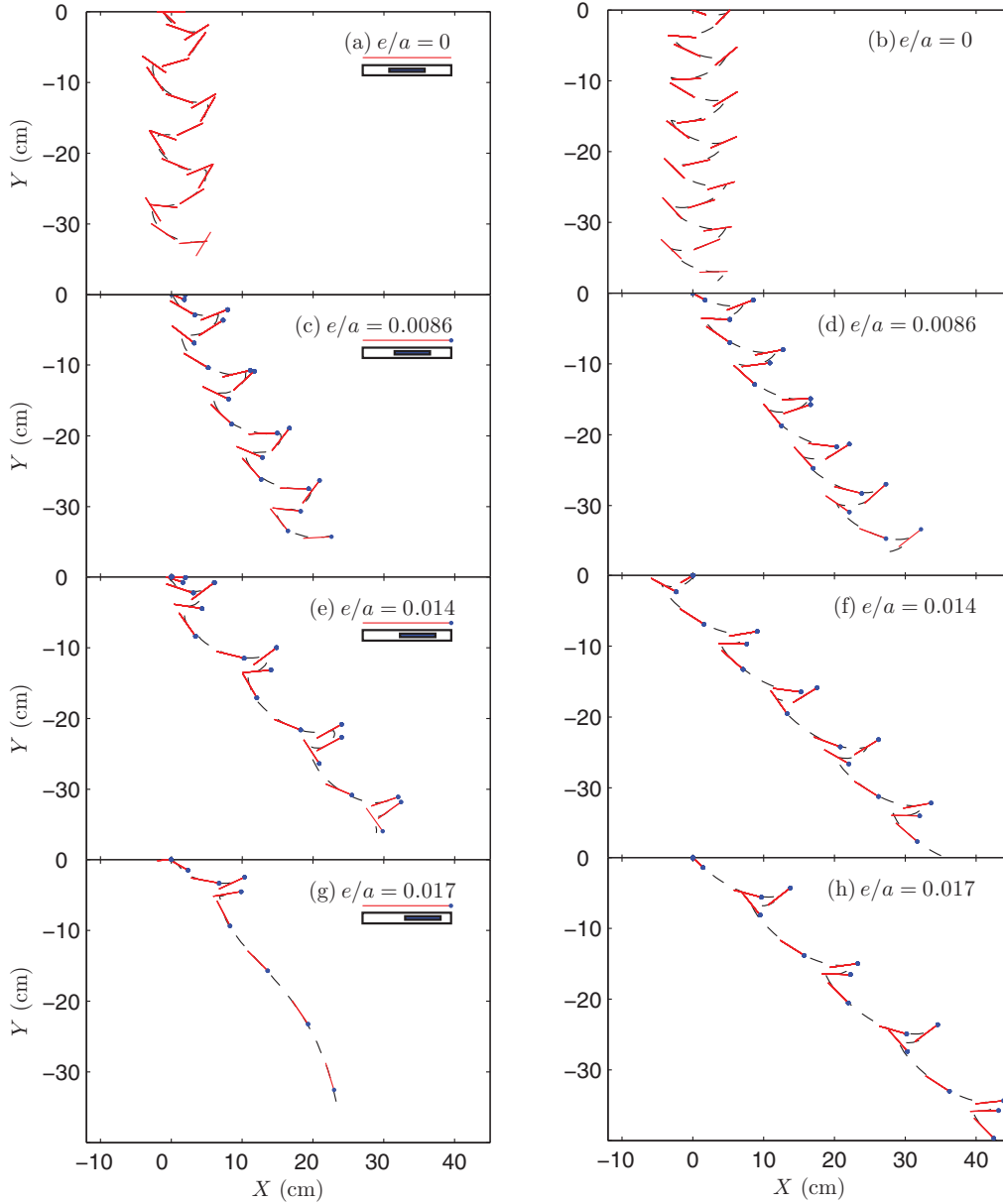


FIG. 3. (Color online) Experimental (left column) and simulated (right column) trajectories (dashed lines) of four plates from Set A with increasing offsets between the centers of gravity and buoyancy. Schematic drawings of plates are shown in the upper right corner of each panel in the left column. Instantaneous positions of plates are shown by short red lines on top of the trajectories of the center of gravity and blue dots denote the direction of the offset.

the assumption that torque generated by aerodynamic lift is negligible in Eq. (7); such an aerodynamic torque has been proven difficult to incorporate in a quasi-steady model [17,29,34].

### B. Temporal dynamics

To understand left-right spatial asymmetry in Figs. 3(c)–3(h), we turn to the plate temporal dynamics. In Fig. 4, we plot the tilting angle  $\theta$  and position ( $X_0$  and  $Y_0$ ) of the center of gravity in the laboratory frame as a function of time for two plates from Set A,  $e/a = 0$  on the left and  $e/a = 0.0143$  on the right. Rotational dynamics, (a) and (b), for both plates is periodic. Let us focus on the period marked by dashed

lines. At time  $t = 2.4$  s, the tilting angle of the zero-offset plate reaches its maximum,  $\theta_{\max} = 1.037$  rad. During the next 0.75 s, the plate rotates clockwise to its minimal tilt angle  $\theta_{\min} = -1.037$  rad; at the same time, the plate moves to the left. Then the plate spends another 0.75 s to reorient back to  $\theta_{\max}$  and to move to the right. At the end of the period, the plate produces no horizontal displacement. However, as shown in Figs. 4(b) and 4(d), the plate with an offset  $e/a = 0.014$  spends more time in the state of counterclockwise (positive) rotation (0.84 s per period) than clockwise (negative) rotation (0.52 s per period), and produces more displacement to the right that leads to a net horizontal translation.

The asymmetry in rotational dynamics originates from the external torque that is produced by buoyancy acting on the

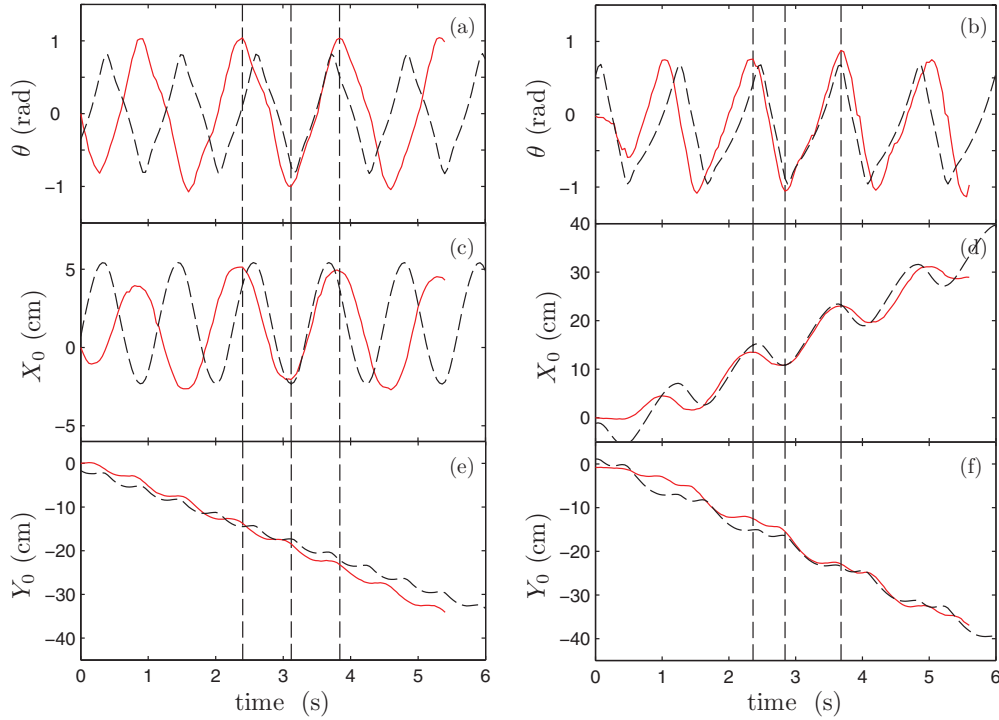


FIG. 4. (Color online) Temporal records for titling angle (top row), horizontal coordinate (middle row), and vertical coordinate (bottom row) for the centers of gravity for a plate with  $e/a = 0$  (left column) and a plate with  $e/a = 0.014$  (right column) from Set A. Experimental and quasi-steady model results are shown by solid and dashed lines, respectively. Simulations reproduce the overall features of experiments but they are different in details.

center of buoyancy and quantified as  $-(\rho_f ab)ge \cos \theta$ , the second term on the right-hand side of Eq. (7). Because the magnitude of plate tilting angle in our experiments is less than  $\pi/2$ , buoyancy, which points upward, produces a negative (clockwise) external torque that speeds up clockwise plate rotation and slows down counterclockwise rotation. We can estimate the magnitude of the offset that is needed to make a difference by balancing two terms in Eq. (7):  $(I + I_a)\dot{\theta}$  and  $\rho_f abge$ . Then we have  $e \sim (I + I_a)\dot{\theta}_{\max}/(\rho_f abg)$ , where  $\dot{\theta}_{\max}$ , the maximal angular acceleration, can be estimated from experimental data in Fig. 4(a). In the end, we get  $e \sim 0.045$  cm that corresponds to  $e/a \sim 2\%$  and lies within the range of our experimental parameters. This approximate calculation supports the idea that a small offset, on the order of a few percent of the plate width, can produce enough torque to qualitatively change the rotational dynamics. To be more quantitative, predictions of the quasi-steady model are plotted as dashed lines in Fig. 4. With the same parameters as in Table II, the quasi-steady model successfully predicts the symmetric dynamics for the zero-offset plate and the spatially-temporally asymmetric dynamics for the plate with a nonzero offset.

Sensitive dependence of falling dynamics on torque has also been reported in recent studies of controlled aerial descent in canopy ants [35] and in bristletails [36]. These studies showed that creatures with very different evolutionary lineage can control their falling trajectories by bending their bodies or rotating their legs. It has been suggested that these changes in the body shape may alter the distribution of drag over different body parts and produce enough torque to affect the trajectories [34,37].

### C. Offset dependence

Besides modifying the rotation speeds, the external torque also changes the mean tilting angle. We averaged  $\theta(t)$  over two full periods and plotted the averaged angle,  $\langle -\theta \rangle$ , in Figs. 5(a) and 5(b) as a function of the offset for all plates in Sets A

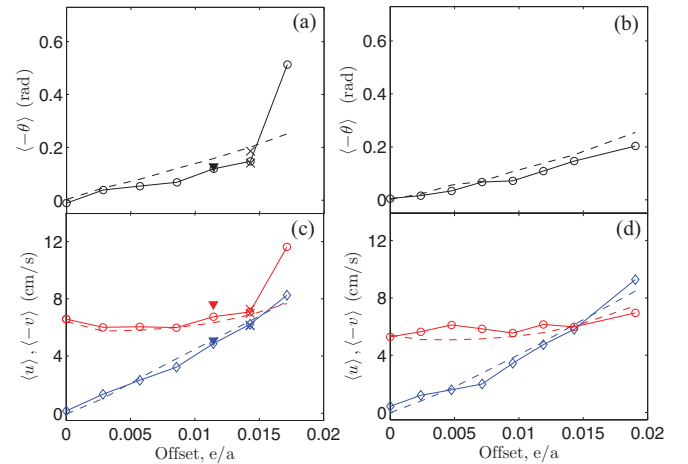


FIG. 5. (Color online) (a),(b) Temporally averaged tilting angle,  $\langle -\theta \rangle$ . (c),(d) Temporally averaged velocities of the center of gravity,  $\langle u \rangle$  (blue diamonds) and  $\langle -v \rangle$  (red circles), as functions of the offset for plates in Set A in the left column and for plates in Set B in the right column. Experimental and model results are shown by symbols and lines, respectively. Crosses in (a) and (c) are results from repeated experiments to show experimental reproducibility. Solid triangles in (a) and (c) are measured with a plate that is 35 cm long in the Z direction.

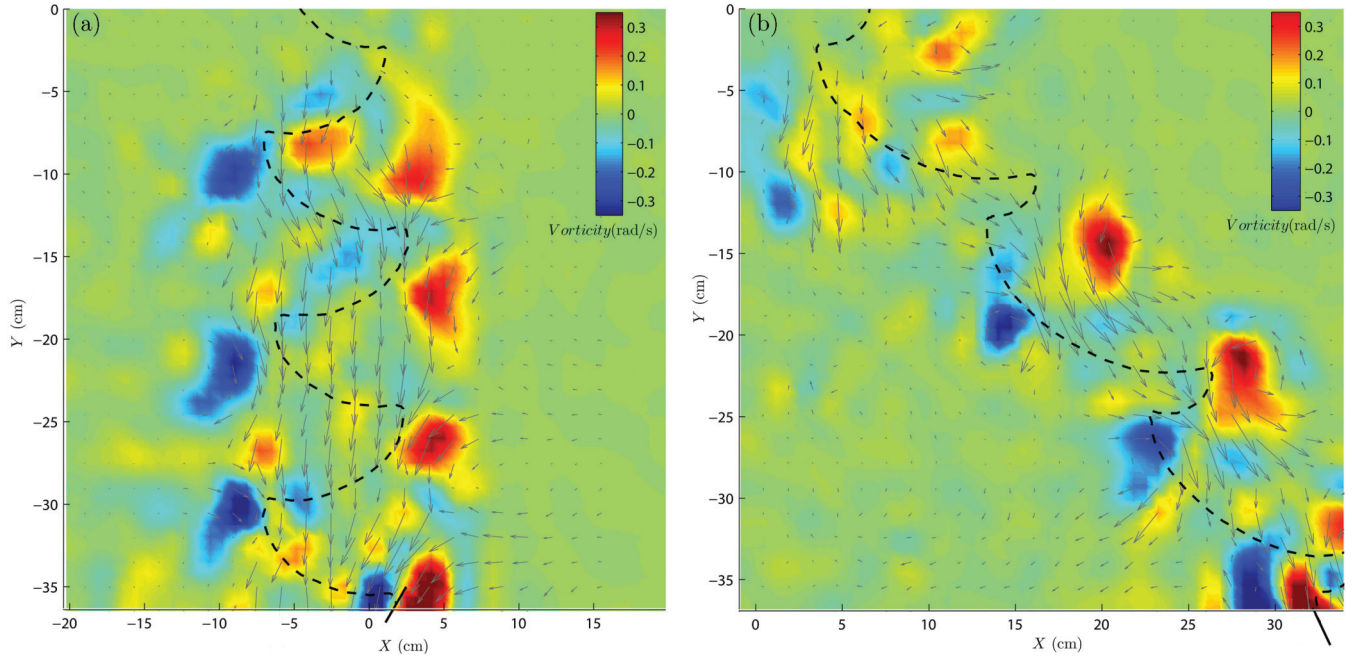


FIG. 6. (Color online) Instantaneous velocity and vorticity fields overlaid with trajectories of two plates from Set A: (a)  $e/a = 0$ , (b)  $e/a = 0.014$ .

and B. Both experiments and models show that, on average, the external torque rotates the plate clockwise and leads to a positive  $\langle -\theta \rangle$  whose magnitude increases with the offset. The sharp increase in  $\langle -\theta \rangle$  seen at the last experimental data point in (a) is caused by the transition to edge-on vertical falling. No such transition has been observed in plates of Set B, possibly because the larger plate width in Set B increases the rotational drag that stabilizes the periodic motion. As shown in Eq. (12), rotational drag depends sensitively on the plate width as  $a^4$ , which means that a 20% increase in  $a$  from 2.5 cm in Set A to 3 cm in Set B leads to a doubling in rotational drag.

To quantify net translational motion, we average the velocities of the center of gravity over two full periods and plot the magnitude of averaged quantities,  $\langle u \rangle$  and  $\langle -v \rangle$ , in Figs. 5(c) and 5(d). Change in the offset has little effect on the vertical falling speed, and horizontal mean speed increases approximately linearly with the offset. While plates in Set A always fall faster than horizontal drift, we see a crossover of  $\langle u \rangle$  and  $\langle -v \rangle$  in Fig. 5(d) at  $e/a = 0.015$ . Also, the last data point in (d) shows a horizontal mean speed that is 50% larger than the vertical mean speed. This demonstrates that a small external torque can be used to generate efficient horizontal motion in falling objects; such a capability may be useful in a few situations, such as plant seed dispersal or glider design.

#### D. Flow fields

Plate motion is closely related to the dynamics of the surrounding fluid. We plot instantaneous velocity and vorticity fields overlaid with plate trajectory in Fig. 6. In (a), we see that a vortex is created and shed when the plate angle reaches its limit value. The shed vortices form a periodic wake synchronized with plate motion. Similar behavior is observed for the plate with  $e/a = 0.014$  in (b); vortices are displaced

horizontally following the plate trajectory. Generated vortices generally stay in the wake behind the plate and no obvious flow features are observed ahead of the plate. This means that the interaction between the plate and the wake it generates is weak, and the plate motion does not depend crucially on its history, supporting the quasi-steady assumption made in the model [17,21,29].

#### IV. CONCLUSION

We have studied the falling dynamics of plates driven simultaneously by an external force and an external torque through laboratory experiments and a quasi-steady model. The magnitude of the torque was systematically varied by changing the offset between the centers of buoyancy and gravity. Torque generated by a small offset on the order of 1% of the plate width can significantly change the rotational dynamics by breaking the symmetry in rotational dynamics and by changing the mean plate orientation. Changes in rotational dynamics then lead to symmetry breaking in the left/right translational motion and cause a net horizontal drift. In experiments with a Reynolds number around 1500, we found that the mean horizontal velocity scales linearly with the offset up to a critical value, beyond which the plate falls vertically in an edge-on configuration. Our study demonstrates that motion of freely moving objects in a fluid, such as that of falling leaves, flying birds, or swimming fish, is sensitive to external torque, and that external torque potentially can be used as an effective control method [34].

#### ACKNOWLEDGMENTS

H.P.Z. acknowledges financial support of the National Natural Science Foundation of China through Grant No.

11104179, of the Shanghai Pujiang Program through Grant No. 12PJ1405400, and of The Program for Professor of Special

Appointment (Eastern Scholar) at Shanghai Institutions of Higher Learning through Grant No. SHDP201301.

- 
- [1] P. Ern, F. Risso, D. Fabre, and J. Magnaudet, *Annu. Rev. Fluid Mech.* **44**, 97 (2012).
- [2] R. List and R. Schemenauer, *J. Atmos. Sci.* **28**, 110 (1971).
- [3] G. Stringham, D. Simons, and H. Guy, US Geological Survey Professional Paper No. 562-c (US GPO, Washington, DC, 1969).
- [4] C. McCutchen, *Science* **197**, 691 (1977).
- [5] R. Dudley, G. Byrnes, S. P. Yanoviak, B. Borrell, R. M. Brown, and J. A. McGuire, *Annu. Rev. Ecol. Evol. Syst.* **38**, 179 (2007).
- [6] J. C. Maxwell, *Cambridge Dublin Math. J.* **9**, 145 (1854).
- [7] G. Kirchhoff, *Collected Work* (Barth, Leipzig, 1882), p. 376.
- [8] H. Lamb, *Hydrodynamics* (Cambridge University Press, Cambridge, 1932).
- [9] V. Kozlov and D. Oniscenko, *Sov. Math. Dokl.* **26**, 495 (1982).
- [10] H. Aref and S. W. Jones, *Phys. Fluids A* **5**, 3026 (1993).
- [11] P. Holmes, J. Jenkins, and N. E. Leonard, *Physica D* **118**, 311 (1998).
- [12] W. W. Willmarth, N. E. Hawk, and R. L. Harvey, *Phys. Fluids* **7**, 197 (1964).
- [13] E. H. Smith, *J. Fluid Mech.* **50**, 513 (1971).
- [14] S. B. Field, M. Klaus, M. G. Moore, and F. Nori, *Nature (London)* **388**, 252 (1997).
- [15] A. Belmonte, H. Eisenberg, and E. Moses, *Phys. Rev. Lett.* **81**, 345 (1998).
- [16] L. Mahadevan, W. S. Ryu, and A. D. T. Samuel, *Phys. Fluids* **11**, 1 (1999).
- [17] A. Andersen, U. Pesavento, and Z. J. Wang, *J. Fluid Mech.* **541**, 65 (2005).
- [18] D. Lentink, W. B. Dickson, J. L. van Leeuwen, and M. H. Dickinson, *Science* **324**, 1438 (2009).
- [19] D. Tam, J. W. M. Bush, M. Robitaille, and A. Kudrolli, *Phys. Rev. Lett.* **104**, 184504 (2010).
- [20] H. J. Zhong, S. Y. Chen, and C. Lee, *Phys. Fluids* **23**, 011702 (2011).
- [21] U. Pesavento and Z. J. Wang, *Phys. Rev. Lett.* **93**, 144501 (2004).
- [22] R. Mittal, V. Seshadri, and H. S. Udaykumar, *Theor. Comput. Fluid Dyn.* **17**, 165 (2004).
- [23] C. Q. Jin and K. Xu, *Commun. Comput. Phys.* **3**, 834 (2008).
- [24] Z. H. Xia, K. W. Connington, S. Rapaka, P. T. Yue, J. J. Feng, and S. Y. Chen, *J. Fluid Mech.* **625**, 249 (2009).
- [25] D. Kolomenskiy and K. Schneider, *Theor. Comput. Fluid Dyn.* **24**, 169 (2010).
- [26] S. Michelin and S. G. L. Smith, *Theor. Comput. Fluid Dyn.* **24**, 195 (2010).
- [27] Y. Tanabe and K. Kaneko, *Phys. Rev. Lett.* **73**, 1372 (1994).
- [28] P. Ern, F. Risso, P. C. Fernandes, and J. Magnaudet, *Phys. Rev. Lett.* **102**, 134505 (2009).
- [29] A. Andersen, U. Pesavento, and Z. J. Wang, *J. Fluid Mech.* **541**, 91 (2005).
- [30] D. Fabre, P. Assemat, and J. Magnaudet, *J. Fluids Struct.* **27**, 758 (2011).
- [31] P. Assemat, D. Fabre, and J. Magnaudet, *J. Fluid Mech.* **690**, 173 (2012).
- [32] L. Sedov, *Two-Dimensional Problems in Hydrodynamics and Aerodynamics* (Interscience, New York, 1965).
- [33] Z. J. Wang, J. M. Birch, and M. H. Dickinson, *J. Exp. Biol.* **207**, 449 (2004).
- [34] P. Paoletti and L. Mahadevan, *J. Fluid Mech.* **689**, 489 (2011).
- [35] S. P. Yanoviak, R. Dudley, and M. Kaspari, *Nature (London)* **433**, 624 (2005).
- [36] S. P. Yanoviak, M. Kaspari, and R. Dudley, *Bio. Lett.* **5**, 510 (2009).
- [37] S. P. Yanoviak, Y. Munk, M. Kaspari, and R. Dudley, *Proc. R. Soc. B* **277**, 2199 (2010).